DOI: 10.1111/cgf.13801

COMPUTER GRAPHICS *forum*
*Volume 00 (2019), number 00 pp. 1–14*

# Automatic Design of Cable-Tensioned Glass Shells

Francesco Laccone[1,2,*], Luigi Malomo[1,*], Maurizio Froli[2], Paolo Cignoni[1] and Nico Pietroni[3]

[1]ISTI – CNR, Italy
francesco.laccone@isti.cnr.it, malomo.luigi@gmail.com, p.cignoni@isti.cnr.it
[2]DESTEC – University of Pisa, Italy
m.froli@ing.unipi.it
[3]University of Technology Sydney, Australia
nico.pietroni@isti.cnr.it

**Abstract**

*We propose an optimization algorithm for the design of post-tensioned architectural shell structures, composed of triangular glass panels, in which glass has a load-bearing function. Due to its brittle nature, glass can fail when it is subject to tensile forces. Hence, we enrich the structure with a cable net, which is specifically designed to post-tension the shell, relieving the underlying glass structure from tension. We automatically derive an optimized cable layout, together with the appropriate pre-load of each cable. The method is driven by a physically based static analysis of the shell subject to its service load. We assess our approach by applying non-linear finite element analysis to several real-scale application scenarios. Such a method of cable tensioning produces glass shells that are optimized from the material usage viewpoint since they exploit the high compression strength of glass. As a result, they are lightweight and robust. Both aesthetic and static qualities are improved with respect to grid shell competitors.*

**Keywords:** physically based modelling, modelling, computational geometry, geometric modelling

**ACM CCS:** • Computing methodologies → Computer graphics; Mesh geometry models

## 1. Introduction

Architectural geometry is an active discipline that is transforming architecture and art: it allows a designer to focus more on the aesthetics relieving him from all other practical considerations and constraints regarding physical realization, such as feasibility, stability, assembly sequence or material usage, which are instead managed by an algorithm in the background.

Architectural design takes advantage of the availability of physical and mathematical foundations to simulate, anticipate and finally optimize the physical behaviour of structures. In recent years, a lot of efforts have been focused on automating the design process of complex architectures, such as free-form vaults, roofs and envelopes. While most of the attention has been focused on structures that use steel or bricks as structural elements (like grid shells [EKS*10, FLHCO10, SS10, ZCBK12] or masonry structures [DPW*14, PBSH13, dGAOD13, WOD09, WSW*12]), little or no attention has been dedicated to structures that employ glass as load-bearing material.

The constant architectural quest for transparency and dematerialization of primary structures and building skins provided a route to appointing glass as a structural material in contemporary buildings. Glass-based constructions could be considered optimal for material usage because they simultaneously offer transparency and excellent structural performances (see Figure 2). However, design and realization involving structural glass are intrinsically challenging due to the fragility of the material, which implies low tensile resistance and sensitivity to peak stress, i.e. due to impacts.

To ensure an adequate safety level, it is necessary to prevent structural glass from carrying tensions or any transverse or torsional loads. While steel can efficiently support both compression and tension, glass structures offer a very high compressive resistance but a limited tensile resistance. Tension favours cracks propagation within the glass and, as a consequence, any small surface defects can

*These authors contributed equally to this work.

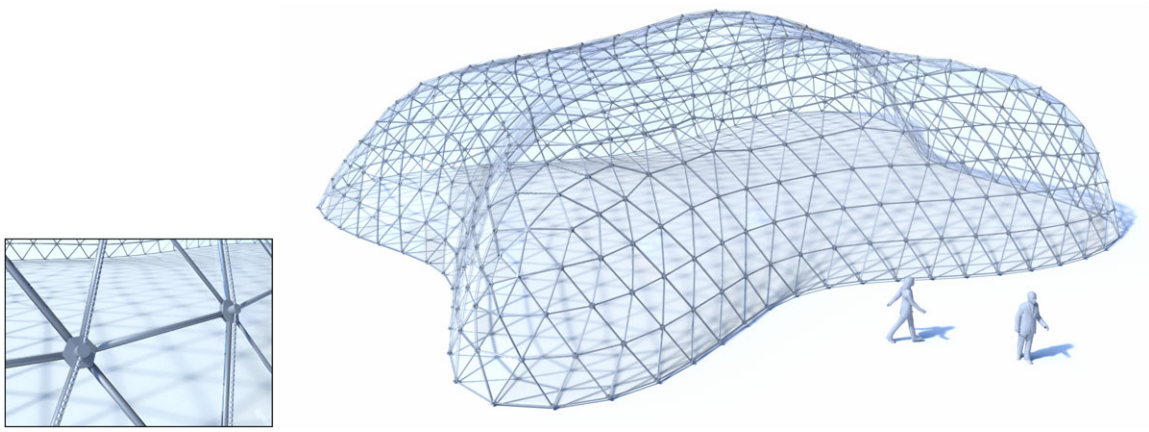

**Figure 1:** *Our method automatically derives a network of tensioned cables to relieve tension from the structure. Thanks to this cable net, we can safely deploy a new type of grid shell that uses its glass panels as a proper structural element.*

quickly degenerate into a severe fracture. Hence, only compressive structures can exploit the structural performance of glass.

Additionally, in the conceptual design phase, we cannot exclude accidental events that could provoke brittle failure of the glass. As a consequence, the structure must be designed to be *safe* for both the occupants and the overall stability of the structure.

We propose a novel method to design grid shells that use glass panels as main structural elements and a very slender network of rods located at their edges for safety reasons. Our method exploits a net of post-tensioned steel cables to superimpose a beneficial compressive stress and mitigate the amount of tension acting on the glass panels.

Using a cable net to reduce tension is a common choice in structural engineering [SS96, RqBJ13, FZG15]. However, the cable layout is usually designed by hand, and the pre-loads are tuned for a specific shape. Instead, we propose the first method for automatic design and optimized tensioning of a cable net. Our framework works on generic single-layer structures and is capable to comply with mechanics and fabrication constraints, such as minimal side length of glass panels and maximum allowable stress. We formulated the problem of deriving an optimized set of cables and their tension as a mixed-integer quadratic problem. Finally, we also validated our results using non-linear finite element analysis (FEM).

Our glass shells exhibit high transparency and apparent immateriality. However, despite their lightness, our structures excel also in static performances.

## 2. Related Work

### 2.1. Structural optimization of grid shells

Grid shells are the discrete version of continuous shell structures, with beams along the edges and panels in place of the faces. Their load-bearing structure is made up of *beams* connected at *joints*, while cladding panels only act as a dead load. In the literature, this kind of structures is usually called *compressive structures*, i.e. the principal stress comes mainly from axial compression forces or compression stresses on a continuous shell.

Geometry plays a fundamental role in the static performance of grid shell structures. A purely compressive grid shell can be obtained only through a form-finding process aimed at finding the *funicular surface* (a surface whose equilibrium is guaranteed by compression-only stresses) that fits with the boundary constraints [BK01, OKF08, OR96]. In this case, an initial form, as designed by an architect, is taken just as a guide to obtain the final structure.

An example of form-finding process designed for masonry is the thrust network analysis [Blo09, PBSH13]. This method has also been extended to the computation of triangular grids in static equilibrium [VHWP12, LPS*13]. Another generation of methods [TSG*14, PTP*15, KPWP17] optimizes the static performance of a grid shell by solely changing the tessellation of the target shape. The idea is to increase the overall rigidity [TPP*16] through a more efficient loads distribution over the beam network. A few recent works also address the realization of torsion-free grid shells structures [PLW*07, PJH*15, TSG*14, JTSW17],

However, most of the methods for grid shell optimization treat axial stress regardless if it is tension or compression. This assumption is generally correct for steel structures, as steel can support any axial load. On the other hand, other materials such as glass can break when subject to significant tensions.

### 2.2. Tension-based structures

One peculiar class of structures that extremize the idea of handling tension forces by relying on cables are Tensegrities [TP03]. Tensegrity structures usually consist of just a set of disjoint struts, tied together by cables connecting their endpoints. In tensegrities, since the design phase, there is a clear separation between elements supporting compression (trusses) and the ones supporting tensions (cables). These structures are mostly known for their desirable


**Figure 2:** *(a) Mock-ups of structures with structural glass[FL18] and (b) arches with structural glass [Sob07].*

aesthetic qualities which have been explored in architecture and art. They can be modelled manually, by assembling pre-computed components [GCMT14], or automatically [Tac13, PTV*17].

Similarly to tensegrity, we strive for structures capable of carrying compression and tension in separate elements. However, our setup is significantly different. Firstly, while tensegrities rely on linear elements only (beams), our structures are composed by piecewise triangular structural elements. Moreover, in our setup, all compressive elements (glass panels) are connected through a network of nodes; as opposite, in tensegrities, each node can connect only one compressive element. Finally, we have no clear separation between compressions and tensions, as we also accept solutions with low tension on panels.

### 2.3. Glass structures

In the last century, glass was extensively employed in architecture; nonetheless, the quest for lightness and immateriality is far from exhausted, and the desire to use glass in even more challenging contexts is growing. This tendency is quite evident with many challenging recent constructions like, e.g. the Zhangjiajie Glass Bridge [Dot16], a 385-m glass-bottomed suspended bridge on the namesake Grand Canyon in China.

A significant advance in this context has been the introduction of large glass panels in architecture that opened the way for their usage as a structural element. From the mechanical point of view, glass is endowed with excellent stiffness and very high compressive strength. It can rely on the absence of viscous, plastic and fatigue phenomena. However, the real behaviour is governed by fragility, which makes it highly risky for challenging purposes, in particular for structural ones.

For structural intents, the design of glass follows principles coming from aircraft engineering, included in the approach known as fail-safe design [HLO08]. Steel elements (bonded or unbonded steel bars) or post-tensioning devices (steel cables or fibres) are usually included as reinforcement to avoid a sudden collapse of cracked glass components. This approach follows the same intuition of reinforced and post-tensioned concrete [Lou11, MCB15, MCB16, EW16].

There are several built structures and real-scale experimental tests in the structural engineering panorama, such as beams, columns and façades. Shells and membranes have attracted less attention so far. We can split glass shells among two categories: those that rely on plate behaviour, where quad or polygonal panels are usually edge-to-edge glued; and those that rely on *strut-and-tie* behaviour, where the panels' vertices are clamped into nodes [BVH10]. The 37 m $\times$ 14 m barrel-vault roof of the *Maximilianmuseum* (Augsburg, Germany) is probably the most ambitious built example of these glass membranes [LW00] that uses a dense cable network and cable spokes. In the conceptual phase of this roof, each panel edge is modelled as a truss (strut if compressed or tie if tensioned), obtaining a structural behaviour akin to a grid shell.

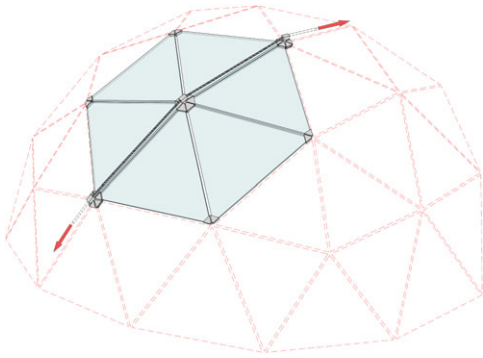

**Figure 3:** *Scheme of post-tensioned steel cable running over the edges of the glass panels.*

The optimization of the post-tensioned glass structure is a new problem in architectural geometry and is centred around two indeterminacies: the optimal cable layout and the optimal pre-loads. In our approach, we considered long sliding cables in order to benefit from simple post-tensioning operations and to obtain small intermediate nodes, and so more transparency (see Figure 3). The cables run along the edges of the glass panels. Each cable has uniform tension and can be either anchored to the ground or form a closed loop on the surface.

## 3. Overview

Given an initial surface, we aim to obtain a shell composed of triangular glass panels and a net of cables with their optimized pre-load. When we deploy these cables, they compress the nodes of the structure to minimize the residual tension on the glass panels and, as a consequence, they also increase the shell's overall robustness. Our processing pipeline can be summarized as follows:

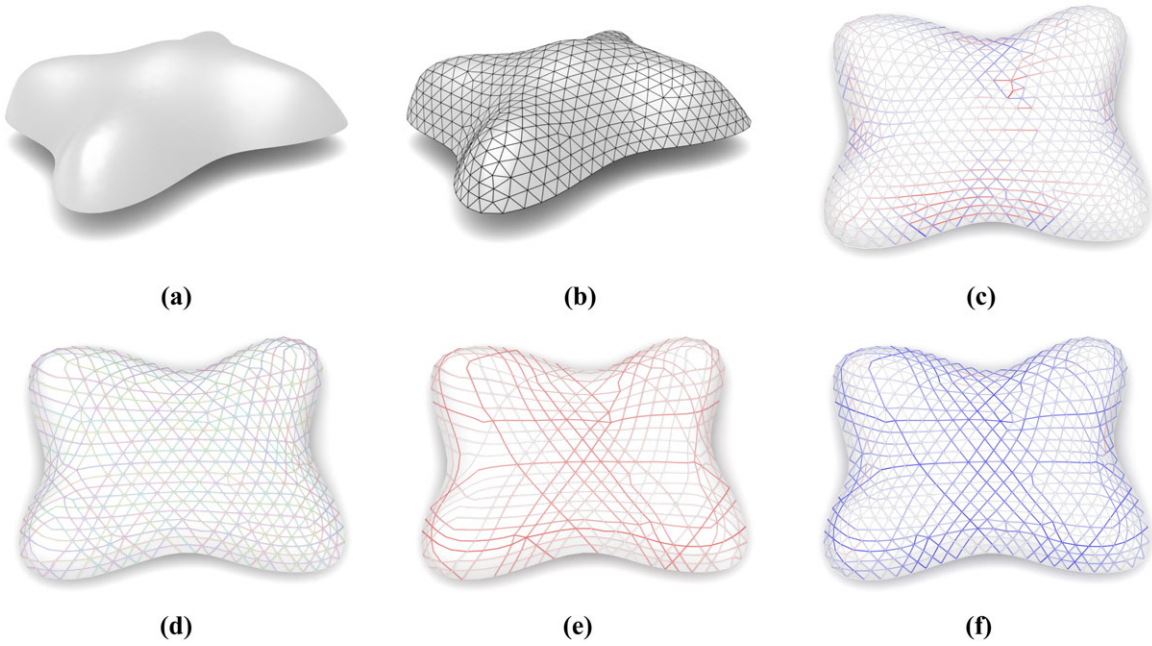


**Figure 4:** *Our processing pipeline shown for the Simplilium case study of Figure 1: (a) the input mesh, (b) the regular re-meshing computed using [JTPSH15], (c) the stress on the linear truss model subject to an external load (blue is compression, red is tension), (d) the candidate cables, (e) the chosen cables and their pre-load and (f) the final stress.*

- we take as input a triangular mesh, with a set of boundary vertices marked as support (Figure 4a);
- we compute a uniform triangular re-meshing using the method of Jakob *et al.* [JTPSH15] (Figure 4b);
- we approximate our shell using a linear truss model, and we compute the stress acting on each truss element when a uniformly distributed load is applied to the structure nodes (Figure 4c);
- we trace a large set of candidate cables: each cable is constrained to follow a sequence of edges of the re-meshed model (Figure 4d);
- we select a small optimized subset of cables and derive appropriate tensions values to reduce the overall tensile stress (Figure 4e).

The final post-tensioned solution has a lower level of tension and improves the static performance of the structure (Figure 4f). We dimensioned every experiment to match with real-world scenarios. This includes the structure overall dimension, the size of glass panels, loads applied and material properties.

We assessed our results by using a professional Finite Element Software [G+D05] to verify the quality and the feasibility of the derived solutions.

## 4. Statics of Our Glass Shells

Our shells consist of an assembly of triangular glass panels, which are both reinforced and post-tensioned in order to provide for an adequate fail-safe behaviour. Thus, if a single panel cracks, the structure is still stable. A set of slender steel rods located at each edge reinforces the overall structure. The role of post-tensioning is played by cables sliding along the edges of the panels [FL18].

From the mechanical point of view, our glass shells can be classified among the class of strut-and-tie structures because they rely on a load transfer mechanism similar to [LW00]. Consequently, we could adopt a simplification in which a piecewise shell is modelled as a truss, whose elements are the edges of the mesh (Section 4.1).

Therefore, in this reduced model, trusses are equipped with an equivalent linear stiffness to mimic the behaviour of the adjacent glass panel edges and its safety steel rod (Section 4.2).

In order to fully capture the mechanical behaviour of our glass shell, we need a complex non-linear FEM where panels are decomposed into several finite elements and contact forces between components are modelled explicitly. Due to its high computational requirements, it is not practical to use this approach inside an optimization process that searches for the best cable net layout. Instead, we use a more straightforward and faster linear analysis (Section 4.3). The fully non-linear FEM (including geometry, contact and material nonlinearities) is used for a final verification step.

### 4.1. Reduced model generation and settings

The proposed framework is based on thin shell theory and is designed for meshes that have prevailing membrane behaviour, as most of the grid shells in architecture. Commonly, grid shells use a beam model with 6 degrees-of-freedom rigid end nodes, which automatically provide both in-plane and out-of-plane resistance. In our case, we adopted a linear truss model, which provides only in-plane resistance. To include the out-of-plane resistance for bending/twisting forces, we added a secondary layer of virtual trusses (crossed blue trusses in Figure 5).

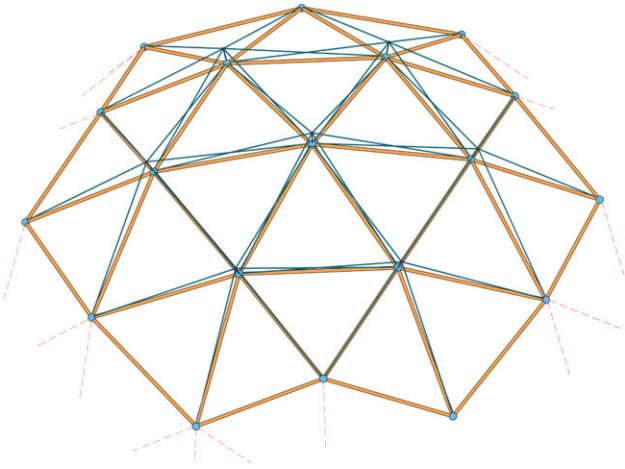

**Figure 5:** *The truss structures (yellow) and the additional trusses (blue) we used to account for non-membrane force components.*

In details, we simulate our glass shell $\mathcal{G}$ as a set of nodes $n_i \in \mathcal{N}$, which are interconnected by a net of linear trusses $t_i \in \mathcal{T}$. The stiffness of each truss $k_i = EA/l_i$, where $l_i$ is the length of the $i$th truss, $E$ is the Young's modulus and $A$, the cross-section area, is computed from the equivalent stiffness (see Section 4.2).

For each node of the main truss $n_i$, we create a dummy node $n_i'$ placed at a short distance along its normal. Each dummy node $n_i'$ is attached both to the original node $n_i$ and to the neighbours of $n_i$ through a set of additional trusses (see Figure 5). Thus, for each edge of the original mesh, there is a single main truss and two crossed additional trusses.

The stiffness of the additional trusses is a small fraction of the one used in the main trusses (0.001%), while the truss along the normal connecting $n_i$ with $n_i'$ has a $10^6$ times the stiffness of the main trusses, so that their relative distance is kept constant during the analysis. Due to their low in-plane stiffness, the additional trusses result almost unloaded under membrane loading, inducing a negligible effect on the accuracy of the simulation. On the other hand, they are essential to avoid local snap of nodes and therefore to satisfy the equilibrium in the presence of out-of-plane loading.

In our shells, the weight of each glass panel is proportional to its area since they all have a constant thickness. We consider a uniform load of 0.4 kN/m$^2$ for 17.52 mm-thick glass panels (laminated heat-strengthened glass pane 8 + 8 mm with 1.52 mm Polyvinyl butyral - PVB - interlayer), 0.1 kN/m$^2$ as reinforcement steel load and an uniformly distributed 1.0 kN/m$^2$ load as a vertical service load (e.g. simulating the effect of a real-life environmental loading such as snow loading). The vertical load finally results in 1.5 kN/m$^2$ and is distributed among nodes proportionally to their Voronoi area [MDSB03]. The supports are pin joints located on each boundary vertex.

Concerning cables, the post-tensioning force is practically generated by a traction force acting on their extremities (i.e. induced by jacks pushing on the extreme anchoring points). As usually done for post-tensioned concrete [Naw00], the pre-load is simulated as an external load: a component acting on extremities and deviation forces. In our model, the former is neglected because it acts on the boundary. Deviation forces are due to change of direction of the cable and are applied at the nodes (Figure 6). In the case of closed loops, only deviation forces occur.

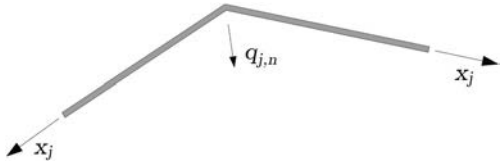


**Figure 6:** *Schematic view of deviation force $q_{j,n}$ acting on the $n$th node due to the $j$th cable (with a constant pre-load of $x_j$).*

Since the cable pre-stress $x_j$ is constant in each cable segment, the node pre-load $q_{j,n}$ is only function of the angle between cable segments: the larger is this angle, the larger is the pre-load magnitude. This node pre-load has components both normal and tangential to the ideal surface, depending on the specific cable path.

### 4.2. Stiffness calibration of the truss elements

To find the parameters of the trusses employed in our reduced model, we built a local non-linear model and examine the response of a single edge shared among two glass panels. The setup includes five steel reinforcement bars which surround two equilateral triangular panels (Figure 7a).

We loaded the central element with either tension or compression forces. The resulting load-displacement curve represents the real interaction between steel and glass with all the expected non-linearities. Then, since the length of the edge $l$ is given, we extracted an equivalent linear stiffness behaviour $E \cdot A$ (where $E$ is the Young's modulus and $A$ the cross-section area) that we used in our linear analyses. The full non-linear response and the equivalent linear truss response are compared in Figure 7(b). We evaluated the stiffness from the exact regression, and then, for the sake of safety, we adopted a reduced stiffness so that the actual forecast displacement for given load of our equivalent truss is smaller than the simulated one in the range of interest, which is on compression side. The adopted value is obtained through the reduction by 20% of the linear regression stiffness achieved in the non-linear model for the reference equilateral panel. The adopted stiffness results on the safe side even if the aspect ratio of the panels is varied at least in the range of interest.

Details on model calibration are included in Appendix A.

### 4.3. Linear finite element analysis

Following the *displacement method*, we formulated the global equilibrium equations in terms of nodal displacements, which represent the solution of the problem. Once displacement is known, and we evaluate the stress of each beam and its axial force by integration. We implemented this linear FEM in MATLAB [MAT18].

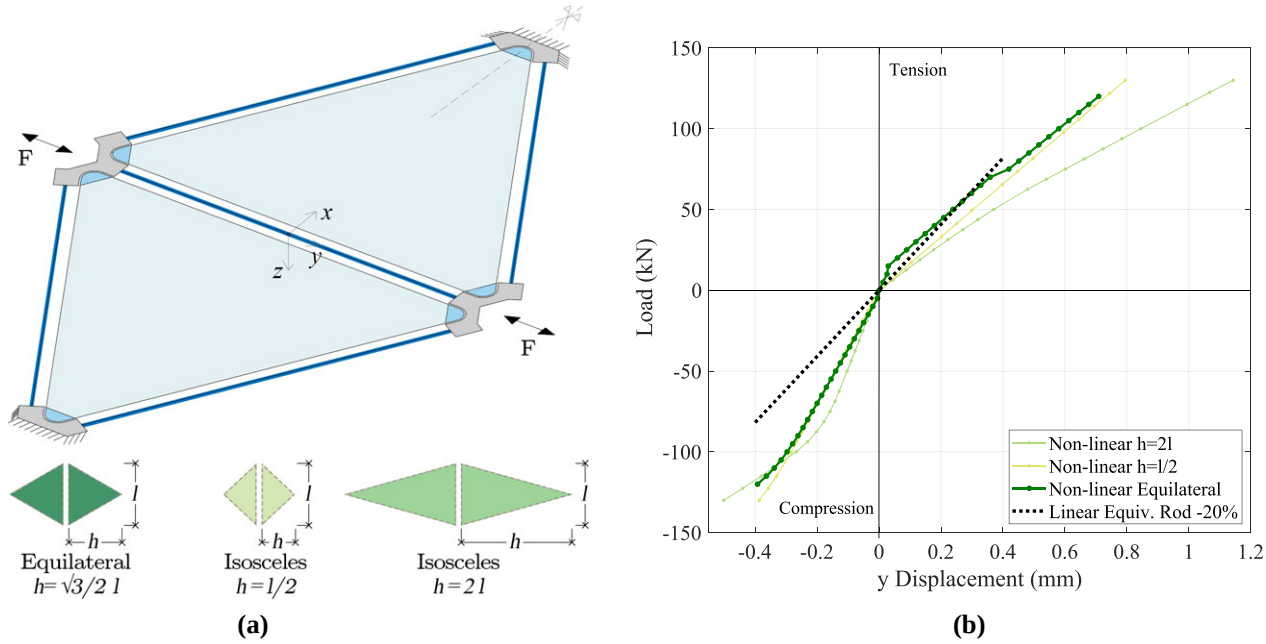


**Figure 7:** *Equivalent truss model: (a) setup used to compute the equivalent truss material properties; and (b) comparison of the displacement obtained by applying axial load on our linear truss with respect to one obtained with the accurate non-linear FEM in the same setup.*

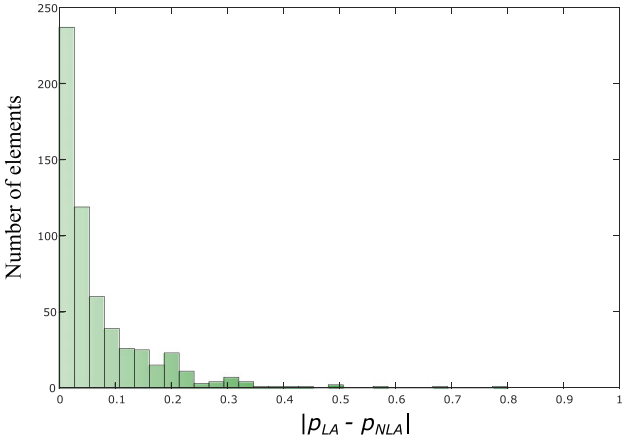


**Figure 8:** *The distribution of the error introduced by our model. This error is measured in terms of difference between normalized displacement computed by our linear FEM $p_{LA}$ and by non-linear model $p_{NLA}$. The displacements have been normalized with respect to their maximum values. Mean of the distribution is 0.0898, and standard deviation is 0.1375. Maximum (non-normalized) displacements are $p_{LA} = 0.0031$ m and $p_{NLA} = 0.0026$ m.*

We compared the response of our linear FEM with a non-linear model developed within a professional software [G+D05]. Figure 8 shows the distribution of displacement error for the *Simplilium* case study (Figure 1) using the linear model with respect to the non-linear FEM when the structure is subject to service load.

Due to the linearity assumption, we evaluate the axial forces resulting from the service load and from each cable load independently. Then, we combined the results following the principle of superimposition of effects. Since displacement is infinitesimal, the superimposition of equilibrium states yields an equilibrium solution. We included details on the linear FEM model formulation in Appendix B.

## 5. Derivation of the Cable Net

Our approach for optimized cable net derivation operates in a discrete setting: in a first step, we build a sufficiently large and well-distributed set of candidate cables $\mathcal{C}$ lying on the surface of the shell, and then we choose the best subset of cables by exploiting the superimposition principle and using a direct constrained optimization solver.

Cables are aligned with other opaque components (e.g. safety bars, glass edges and seals) for aesthetic reasons, to reduce their

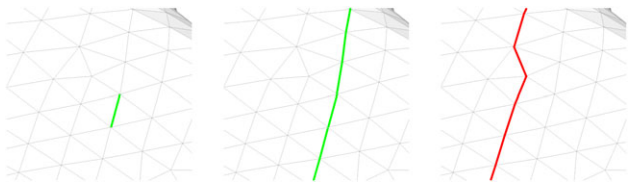

**Figure 9:** *Left: the re-meshed shell with an edge to be traced. Centre: a traced candidate cable. Right: a cable that has been discarded because of an abrupt change of direction.*

visual impact, and for structural reasons. Indeed, if a cable crosses panels, it might introduce undesired bending loads.

Because of this alignment, the cables and the triangular panels layout are then strictly related, both geometrically and structurally. Hence, our first step is computing a good, regular, appropriately sized, triangular meshing of the initial surface using the method in [JTPSH15]. For all the examples shown in this paper, we used a target edge length of 1 m.

Cable paths are then generated by iteratively joining adjacent edges having closest directions (Figure 9), until all edges of the mesh are explored. A cable can either terminate at the border or create a loop.

Each resulting polyline corresponds to a candidate cable $c_j$. Each candidate cable should be as smooth as possible for efficiency (see Section 4.1), so we discard from the candidate cables $\mathcal{C}$ the ones that include kinks with a deviation angle larger than 40°.

### 5.1. Selection of the optimized subset of cables

Given a glass shell $\mathcal{G}$ and a service load that the structure must withstand, we seek an optimal subset of cables $C$ with their corresponding pre-loads $x_j$ that minimize overall positive tension. In particular, we minimize the strain energy of tensile-stressed trusses only, $U^+$.

Given the strain energy of the $i$th truss $U$,

$$\begin{aligned} U &= \frac{1}{2} \cdot (A \cdot \sigma) \cdot (\epsilon \cdot l) \\ &= \frac{1}{2} \cdot \sigma^2 \frac{A}{E} \cdot l \\ &= \frac{1}{2} \cdot \frac{N^2}{EA} \cdot l, \end{aligned}$$

where $A$ is the truss cross-section, $\sigma$ and $\epsilon$ are stresses and strains, respectively, $l$ is the truss length, $E$ is the Young's modulus and $N$ is the axial force. We want to minimize the amount of strain energy relating to tensile-stressed trusses only,

$$U^+ = \sum_{i^+} \frac{1}{2} \frac{N_i^2}{EA} \cdot l_i,$$

where $i^+$ is the subset of trusses in which the axial force $N > 0$ (i.e. $\sigma > 0, \epsilon > 0$).

Using our linear FEM, for each truss $t_i$, we define as $g_i$ its axial force resulting from the service load on $\mathcal{G}$. We derive the stresses by using the displacement method as shown in Appendix B.

We characterize the glass structure response when we apply a tension on each cable independently. More precisely, we define as $s_{ij}$ the axial force arising on truss $t_i$ when we deploy a unitary pre-load on the cable $c_j$, i.e. 1 kN. Note that in this setup, apart from the cable loading, neither gravity nor other external loads occur.

Due to linearity assumption, the $s_{ij}$ term will be linearly related to the pre-load, $x_j \geq 0$, applied on its respective cable $c_j$. Thus, the resulting axial force will be $x_j \cdot s_{ij}$.

For the superimposition principle, the effect of each cable is independent and it can be linearly summed, together with forces $g_i$ induced by the given load. The resulting axial force of $t_i$ yields:

$$N_i = g_i + \sum_j x_j \, s_{ij}.$$

Since the equilibrium is guaranteed in each solution, by summing each force contribution, we preserve the static equilibrium of $\mathcal{G}$. The optimization can be written as:

$$\min \sum_{i^+} \frac{1}{2} \frac{N_i^2}{EA} \cdot l_i. \tag{1}$$

To select the cables and optimizing their pre-loads $x_j$, we model the minimization in Equation (1) as a mixed-integer quadratic formulation using Gurobi [GO18]. In particular, we solve:

$$\arg\min_x \sum_i \frac{1}{2} \frac{m_i^2}{EA} \cdot l_i \tag{2}$$

s. t.

$$\begin{aligned} &0 \leq x_j \leq \gamma && \forall c_j, \\ &0 \leq m_i && \forall t_i, \\ &\omega \leq g_i + \sum_j x_j \, s_{ij} \leq m_i && \forall t_i, \end{aligned}$$

where $m_i$ is an additional variable that represents the positive axial force acting on $t_i$. In particular, since we minimize over $\sum m_i^2$, we have $m_i = \max(N_i, 0)$.

The value $\gamma$ is a constant parameter that defines the maximum pre-load of cables; $\omega$ is a constant parameter defining the maximum axial compression that each truss can withstand.

Additionally, to accommodate aesthetic, mechanical and assembling needs, we generate a set of conflicting cable pairs $\mathcal{K}$. When two cables are conflicting, they cannot be selected contemporarily in the final solution. To account for conflicts, in our mixed-integer formulation, we add a boolean variable $b_j$ for each cable $c_j$ to indicate whether a candidate cable is selected in the final solution, i.e. we force $x_j$ to be zero when also $b_j$ is zero. Then, for each conflict pair, $\{c_{j_1}, c_{j_2}\} \in \mathcal{K}$, we add a linear constraint $b_{j_1} + b_{j_2} \leq 1$.

As explained, the minimization objective models the total strain energy relative to positive axial forces only. The truss properties $E \cdot A$, Young's modulus and cross-section area are constant and can be neglected. Thus, our formulation becomes:

$$\arg\min_x \sum_i m_i^2 \cdot l_i \tag{3}$$

s. t.

$$\begin{aligned} &0 \leq x_j \leq \gamma && \forall c_j, \\ &b_j = 0 \quad \Rightarrow \quad x_j = 0 && \forall c_j, \\ &0 \leq m_i && \forall t_i, \\ &\omega \leq g_i + \sum_j x_j \, s_{ij} \leq m_i && \forall t_i, \\ &b_{j_1} + b_{j_2} \leq 1 && \forall \{c_{j_1}, c_{j_2}\} \in \mathcal{K}. \end{aligned}$$

**Table 1:** *Results of our optimization on different models: the name of the model (see Figure 11); number of vertices $|V|$; number of faces $|F|$; the size of the axis aligned bounding box in metres; the total load comprehending structure weight and applied load (in tons); the total positive strain energy before the optimization $T_0$ and after $T_{opt}$; the total reduction; the linear buckling multiplier before $\lambda_0$ and after the optimization $\lambda_{opt}$; the time required by the optimization process.*

| | $\|V\|$ | $\|F\|$ | Size $w\times d\times h$ (m) | Load (tons) | $T_0$ | $T_{\text{opt}}$ | Cut | $\lambda_0$ | $\lambda_{\text{opt}}$ | Time (s) |
|---|---|---|---|---|---|---|---|---|---|---|
| Simplilium | 582 | 1090 | 25.7×24.2×6.3 | 75.6 | 7443.75 | 477.45 | 94% | 9.74 | 15.22 | 6.41 |
| Vault | 506 | 931 | 19.1×20.3×6.9 | 56.4 | 6485.41 | 56.44 | 99% | 9.11 | 14.69 | 24.90 |
| Bean | 429 | 796 | 21.7×16.7×5.7 | 52.8 | 187.86 | 23.49 | 87% | 11.72 | 19.12 | 7.64 |
| Calla | 557 | 1036 | 20.8×16×8.6 | 58.8 | 1354.57 | 27.49 | 98% | 10.57 | 17.91 | 9.47 |
| Snake | 456 | 829 | 26.8×14.6×6.4 | 53.3 | 1359.29 | 0.00 | 100% | 10.16 | 15.85 | 8.92 |
| Hole | 489 | 909 | 19.4×17.3×3.6 | 52.7 | 1675.75 | 22.40 | 99% | 19.62 | 32.12 | 10.82 |
| Triangle | 614 | 1155 | 25.9×20.9×8 | 75.7 | 681.33 | 0.00 | 100% | 8.90 | 13.97 | 8.47 |

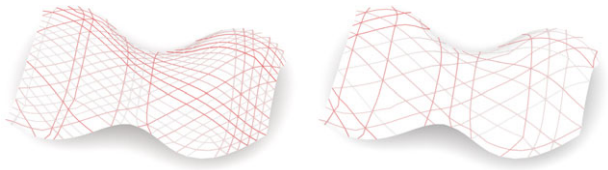


**Figure 10:** *A set of linear constraints can be used to impose a minimum distance between cables. Distances are expressed as % of the diagonal of the axis aligned bounding box.*

Boolean variables enable the user to include a variety of additional constraints, e.g. setting up a maximum number $C_m$ of employed cables ($\sum b_i \leq C_m$), matching global constraints such as symmetry in the selection of cables or a minimal distance between them (see Figure 10). In our setup, since it is possible for two different candidate cables to share some edges (see Section 5), we adopted conflict pairs to avoid overlapping cables.

## 6. Results and Discussion

We tested our algorithm on several datasets (see Figure 11). We dedicated special attention to fit our experiments to real-world scenarios. Size, weight and applied load of each structure are dimensioned to match a plausible glass shell that can be safely deployed.

For all our experiments, we employed glass panels with 17.52 mm of thickness (laminated heat-strengthened glass pane 8 + 8 mm with 1.52 mm PVB interlayer) and safety steel bar (reinforcement) with a hollow profile with 33.7 mm of diameter and 4 mm of thickness. To avoid local buckling failures, we limited the maximum compression for the truss in the reduced linear model to $\omega = -30$ kN. For post-tensioning, we employed steel cables with 15 mm of diameter and set their maximum tension to $\gamma = 40$ kN. Apart from collaborating with glass in structural terms, the rods assembly forms a skeleton that facilitates the assembly phases and prevents the structure from collapsing in the unfortunate case of damage to a glass panel.

The test results are collected in Table 1. The derivation of the optimized cables layout uses Gurobi [GO18] for constrained energy minimization, and it took up to 25 s to run on a i7-6920HQ 2.9Ghz Mac. Our method can achieve an impressive reduction of the overall tension energy on the glass shell (from 87% to 100%).

We increased the overall robustness of the structure as demonstrated by the gain in linear buckling multiplier $\lambda$. The buckling multiplier measures the ability of a structure to bear the applied load (equal to a uniformly distributed load in this case) before collapsing for instability. In structural engineering, the buckling multiplier is universally considered as a measure of the robustness, especially in the case of compressive structures, and therefore it should be ideally maximized.

We validated our results using a professional software [G+D05] by performing non-linear FEM analysis of the accurate model plugging in the pre-loads obtained from the optimization (Figure 12, middle). As a proof of the accuracy of the selected pre-loads, we increased their values artificially in the non-linear model. We might think that once we found the cables and their pre-loads, an increase in cable pre-loads will induce an additional beneficial reduction of the overall tension in the structure. We demonstrated in Figure 12 that this intuition is instead wrong and the pre-loads found by the algorithm represent an optimized solution.

The non-linear analyses consider large displacements and contact nonlinearities; however, materials adopt linear behaviour with characteristic values according to the global modelling approach of [FLM17], which basically is akin to that adopted for the stiffness calibration Section 4.2). Major differences are the nodes, which are simplified as dimensionless elements, and the contact between nodes and panels corner, which is simulated through a calibrated cutoff element. Mesh quality analysis and convergence of the non-linear analysis are shown in Figure 13.

We compared our structures with typical grid shells where steel is the only load-bearing material (see Figure 14). To achieve comparable static performance, we tried to match the same buckling multiplier of our glass shells ($\lambda_{\text{opt}}$) by only relying on structural steel. Practically, using the same non-linear FEM model, we converted structural glass panels into dead loads applied at the nodes, and the reinforcement rods forming a skeleton into a more

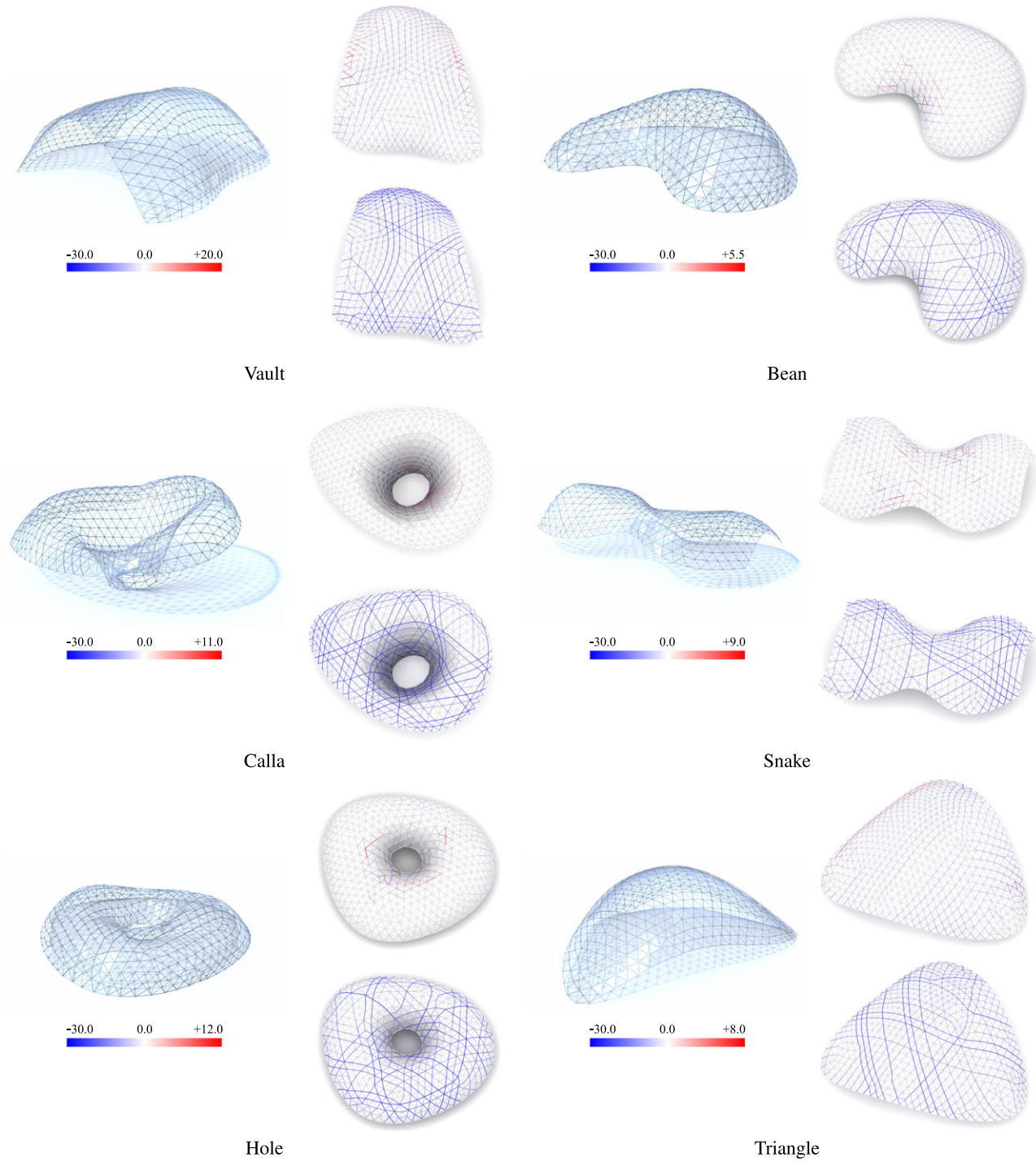


**Figure 11:** *For each model, we show that the tension before and after the cable net has been deployed with the proper tension (red corresponds to tensions and blue to compressions).*

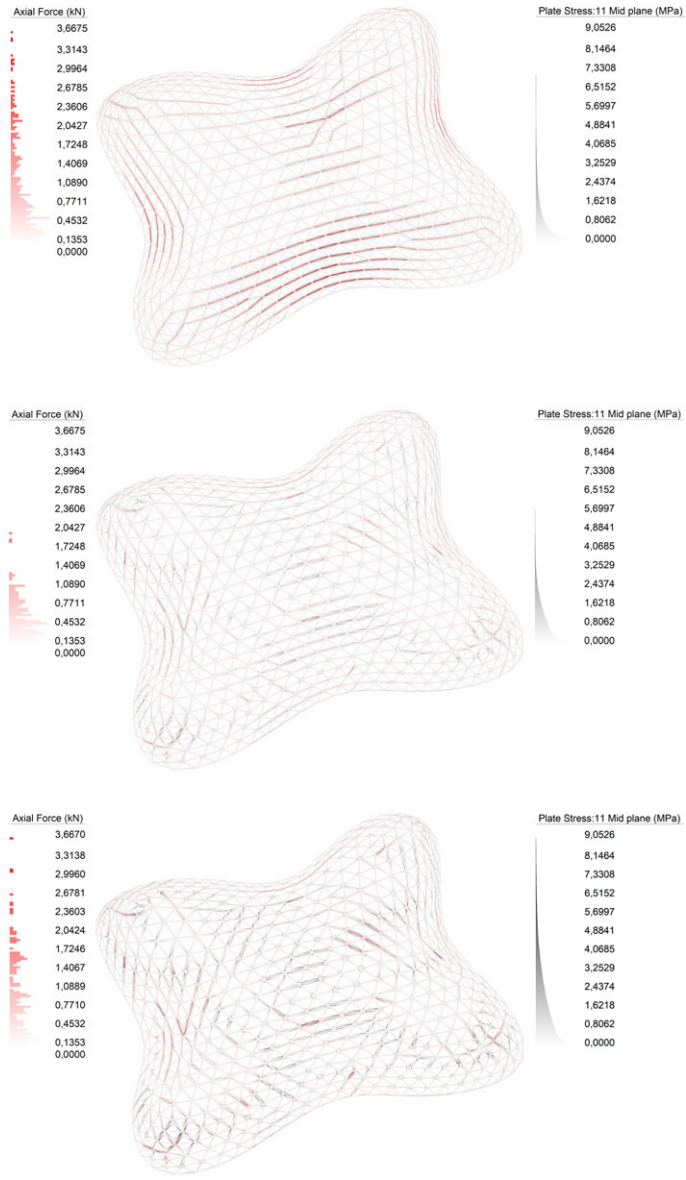


**Figure 12:** *Non-linear FEM analysis visualizing tensions acting on the safety beams (left legend) and on the glass panels (right legend). Top: performed on glass shell without post-tensioned cables; middle: including post-tensioned cables; bottom: the final tensions of the structure when cable tension is artificially multiplied by 1.5.*

stiff network. We manually match the buckling factor by changing cross-section properties of the steel network. This is a non-trivial task; therefore, we performed this validation only for a few models.

Using hollow steel beams, we can tune both the outer diameter and thickness. Usually, we obtained comparable performances if the diameter is doubled. In this case, the total weight is also roughly doubled, and the overall transparency of the structure will be inevitably affected by the new size of the beam, see Figure 14.

Using solid steel beams, instead, we can benefit from a smaller cross-section, which is still bigger than ours, and the total weight of the steel will be roughly quintupled. Our shells, making use of glass structurally, demonstrate advantages concerning both visual and structural lightness, thanks to, respectively, the small impact on transparency and the high ratio between load capacity and own weight.

On the computational side, the truss model not only constitutes an acceptable representation of our scenario and is suitable for the conceptual design of post-tensioned glass shells, but also guarantees

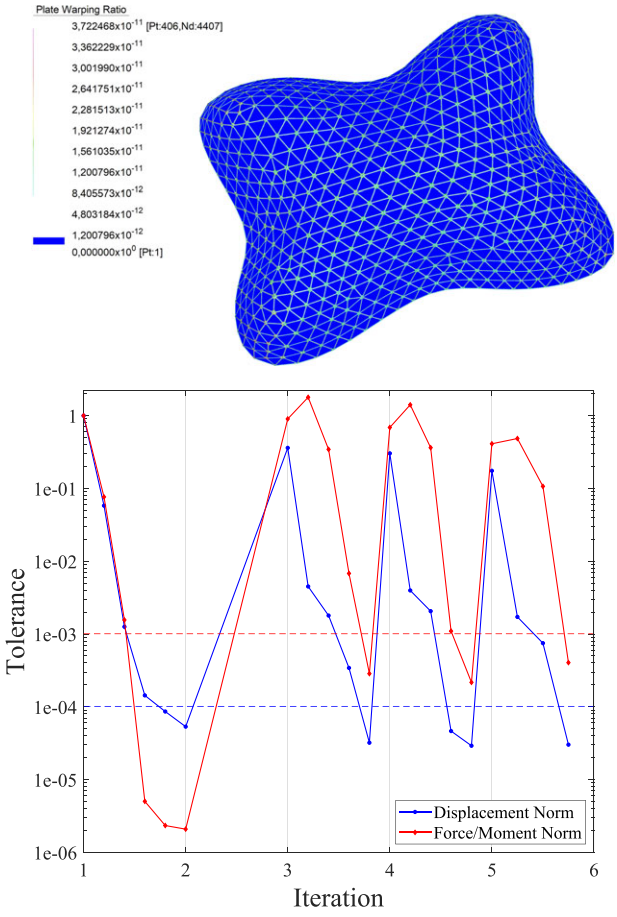


**Figure 13:** *Mesh quality analysis (top) and convergence plot (bottom) of non-linear FEM (Simplilium case). The service load occurs at iteration 4.*

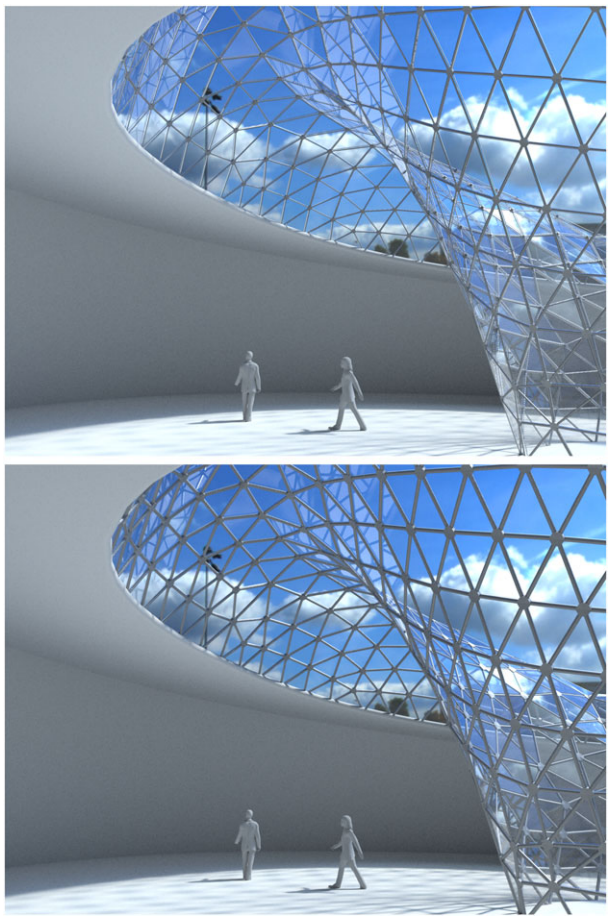

**Figure 14:** *A comparison between our post-tensioned glass shell (top) and a classical grid shell with same tessellation and comparable buckling factor (bottom). Hollow steel beams of* 63.5 *mm outer diameter and* 4 *mm thickness are used for the grid shell (double section with respect to our case).*

a fast solution. Indeed, we can easily superimpose forces and test various loading effects. This procedure leads to structural-effective cable layouts, as confirmed by the results shown in Figures 12 and 14 and Table 1.

We would like to remark that our method is sensitive to any changes in the boundary conditions. Changing the shape or the external loads can alter the space of possible equilibrium configurations. As a consequence, the minimization of the total strain energy can converge to a different solution, and the chosen subset of cables can change accordingly.

Besides, our method is also dependent on the initial meshing. Indeed, the initial tessellation uniquely determines both the position of the linear structural element and the possible cable paths. Hence, to keep a tractable formulation of the problem, we choose to preserve both the original shape and the tessellation during the entire optimization process. The limitation mentioned above, however, allows for a more practical, simple and stable formulation.

To obtain a regular initial tessellation, we initially perform a re-meshing using instant meshes [JTPSH15]. However, different re-meshing algorithms can also be successfully employed.

## 7. Conclusions

We presented a novel algorithm for the automatic design of architectural shells composed by structural glass panels. Given an input surface, our approach generates a feasible panel tessellation of the surface enriched by an optimized cable layout, which can release the glass panels from tension and increase the overall robustness of the shell. As a result, we can safely adopt glass panels as structural elements to support compression forces. Moreover, limiting compression with a lower boundary, the material is not only used for its most suitable and reliable structural characteristics, but it is optimally employed and more uniformly loaded.

We believe that our method could inspire architects to explore the power of glass as a structural element for the construction of a new generation of transparent shells.

We demonstrated the effectiveness of our method with several application scenarios. We accurately tuned and dimensioned each experiment to match with real-world architecture so that the simulation could reflect realistic cases. The main limitation of our method

is that it can only be applied to input surfaces that are funicular or almost-funicular, namely without significant out-of-plane loads (such as bending or twisting).

Our cable placement strategy can be generalized to design tension layouts for a broader class of structures. Further improvements of the method can provide more degrees of freedom on cable placement, for example, by placing the cable at an arbitrary distance along the surface's normal to release it from the bending. Thus, also shape limitation could be overcome. Another possibility is allowing the cables to cross the panel tessellation under the choice of different, non-modular, construction materials that still become critically fragile under tensions.

**Acknowledgements**

This research was partially funded by the Italian PRIN project DSurf (grant no. 2015B8TRFM).

**Appendix A: Details on Stiffness Calibration of Linear Truss**

To calibrate the equivalent stiffness of the main trusses, to be used in our linear FEM, we build a non-linear model using the professional package Straus7 [G+D05]. This model includes a base unit of the structural system made up of two equilateral triangular panels (laminated heat-strengthened glass pane $8 + 8$ mm with 1.52 mm PVB interlayer) surrounded by five reinforcement bars (hollow steel profile of 33.7 mm outer diameter and 4 mm thickness), see Figure 7(a).

To obtain the non-linear force–displacement relation, from which the equivalent stiffness is calibrated, we subject the inner nodes of the base unit to increasing tension and compression edge-aligned in-plane forces ($F$ in $y$ direction of Figure 7a) up to tensile or buckling failure, respectively.

The non-linear model uses physically based properties that are derived from full-scale experimental tests made on glass–steel beam specimens, which are mechanically akin to the present system. The detailed modelling level from [FLM17] is adopted. Glass is modelled as eight-node quadrilateral FE (Quad8) of approximate size of 5% of the panel side length. Steel reinforcements are modelled as two-node beams. Steel nodes, where rods and beams merge, are modelled as thick steel plates. The glass-to-steel contact is considered in the present case by including the behaviour of the spacers through compression-only cut-off bars, arranged radially to the rounded glass corners. All materials have linear elastic properties with characteristic values, except for the cut-off bars that have compression-only linear behaviour with brittle failure at 5 KN and the stiffness of the aluminium, which is the material used for spacers. The analysis considers large displacement.

We used the exact regression of the force–displacement plot for case of the equilateral triangle, and then we applied the homogenized section method to find the equivalent properties of a linear truss having same stiffness $E \cdot A$ (the length of the edge $l$ is given). This value has been reduced by 20% to be on the safe side. Finally, adopting the Young's modulus of steel $E = 210$ GPa, we obtained an equivalent cross-section area $A = 10\ \text{cm}^2$. These are the parameters that we employed for our main trusses.

**Appendix B: Details on Linear Truss Model**

The truss model is a linear FEM created using MATLAB [MAT18]. We implemented an explicit solver based on the displacement method with the hypothesis of infinitesimal displacement, i.e. where the equilibrium of the structure is formulated in its undeformed state.

The final aim is to evaluate displacements, reactions and forces at elements, which form altogether a three-dimensional truss structure where all loadings are applied at the nodes. In our setup, each mesh edge is a two-nodes truss element with three translational degrees of freedom per node (in the global reference system), whose axial stiffness $k = E \cdot A/l$ matches the equivalent truss stiffness (dashed line in Figure 7b).

The solutions of the problem are nodal displacements, which are evaluated by solving the matrix problem:

$$\mathbf{Kp} = \mathbf{q},$$

where $\mathbf{K}$ is the stiffness matrix that stores known constants and is a function of the geometry and the material properties; $\mathbf{p}$ is the vector of unknown displacement and $\mathbf{q}$ is a vector of known nodal loads. Several solutions are derived, one for each load vectors, $q = q_0$ for the service load and $q = q_j$ for each $j$th cable load.

Once the displacement vector $\mathbf{p}$ is known, the stress vector can be easily computed due to the linear relationship between strains and stresses $E \cdot \epsilon = \sigma$. For each element, the axial forces are derived from integration of the stress over the cross-section area $A$. The vector $g$ derives from the load case $q = q_0$; and vectors $s_j$ derive from the load cases $q = q_j$.

The total strain energy (Equation (B.1)) is computed in each load scenario.

$$U = \sum_i \frac{N_i^2}{EA} \cdot l_i. \tag{B.1}$$

As hinted in Section 4.1, in our linear FEM, we can decouple the membrane behaviour, namely axial forces on the main trusses, and the out-of-plane behaviour (axial forces on additional trusses). In our setup, the energy of the main trusses $U_{\text{main}}$ and the energy of additional trusses $U_{\text{add}}$ are evaluated separately and compared. To discard solutions that potentially invalidate the base hypotheses (i.e. prevailing membrane behaviour), we firstly examined the obtained displacement field, checking if the truss manifests snapped nodes, and secondly we measured the strain energy ratio $u = U_{\text{add}}/U_{\text{main}}$. In particular, we verify that $u \leq 1\%$ for a given load. If so out-of-plane components (additional trusses) are correctly deemed scarcely used.

The cable load $q = q_j$ includes deviation forces applied at nodes (on which the cable $c_j$ is supposed to be installed) generated by a unitary pre-load of 1 kN. Its effect on the $i$th truss is expressed as $s_{i,j}$. Due to the linearity of the problem, if the pre-load is increased to $x_j \cdot 1$ kN (where $x_j \geq 0$), the resulting axial force will be simply $x_j \cdot s_{ij}$ with no need for a new analysis.

## References


[BK01] Bulenda T., Knippers J.: Stability of grid shells. *Computers & Structures 79*, 12 (2001), 1161–1174. https://doi.org/10.1016/S0045-7949(01)00011-6.

[Blo09] Block P.: *Thrust Network Analysis: Exploring Three-Dimensional Equilibrium*. PhD thesis, Massachusetts Institute of Technology, 2009. URL: http://hdl.handle.net/1721.1/49539. Accessed: 2018-06.

[BVH10] Bagger A., Verhegghe B., Hertz K. D.: Modeling plate shell structures using pyformex. In *Symposium of the International Association for Shell and Spatial Structures (50th 2009 Valencia). Evolution and Trends in Design, Analysis and Construction of Shell and Spatial Structures: Proceedings* (2010), Editorial Universitat Politècnica de València. URL: http://hdl.handle.net/10251/6949. Accessed: 2018-06.

[dGAOD13] de Goes F., Alliez P., Owhadi H., Desbrun M.: On the equilibrium of simplicial masonry structures. *ACM Transactions on Graphics 32*, 4 (July 2013), 93:1–93:10. https://doi.org/10.1145/2461912.2461932.

[Dot16] Dotan H.: Zhangjiajie grand canyon glass bridge. *Challenging Glass Conference Proceedings 5* (2016), 3–12. https://doi.org/10.7480/cgc.5.2290.

[DPW*14] Deuss M., Panozzo D., Whiting E., Liu Y., Block P., Sorkine-Hornung O., Pauly M.: Assembling self-supporting structures. *ACM Transactions on Graphics 33*, 6 (November 2014), 214:1–214:10. https://doi.org/10.1145/2661229.2661266.

[EKS*10] Eigensatz M., Kilian M., Schiftner A., Mitra N. J., Pottmann H., Pauly M.: Paneling architectural freeform surfaces. *ACM Transactions on Graphics 29*, 4 (July 2010), 45:1–45:10. https://doi.org/10.1145/1778765.1778782.

[EW16] Engelmann M., Weller B.: Post-tensioned glass beams for a 9 m spannglass bridge. *Structural Engineering International 26*, 2 (2016), 103–113. https://doi.org/10.2749/101686616X14555428759000.

[FL18] Froli M., Laccone F.: Static concept for long-span and high-rise glass structures. *Journal of Architectural Engineering 24*, 1 (2018), 04017030. https://doi.org/10.1061/(ASCE)AE.1943-5568.0000285.

[FLHCO10] Fu C.-W., Lai C.-F., He Y., Cohen-Or D.: K-set tilable surfaces. *ACM Transactions on Graphics 29*, 4 (July 2010), 44:1–44:6. https://doi.org/10.1145/1778765.1778781.

[FLM17] Froli M., Laccone F., Maesano D.: The TVT Glass Pavilion: Theoretical study on a highly transparent building made with long-spanned TVT portals braced with hybrid glass-steel panels. *Buildings 7*, 2 (2017), 50. https://doi.org/10.3390/buildings7020050.

[FZG15] Feng R.-Q., Zhang l., Ge J.-M.: Multi-objective morphology optimization of free-form cable-braced grid shells. *International Journal of Steel Structures 15*, 3 (September 2015), 681–691. https://doi.org/10.1007/s13296-015-9014-6.

[GCMT14] Gauge D., Coros S., Mani S., Thomaszewski B.: Interactive design of modular tensegrity characters. In *Eurographics/ACM SIGGRAPH Symposium on Computer Animation* (2014), V. Koltun and E. Sifakis (Eds.), The Eurographics Association. https://doi.org/10.2312/sca.20141131.

[G+D05] G+D Computing: Straus7, 2005.

[GO18] Gurobi Optimization L.: Gurobi optimizer reference manual, 2018. URL: http://www.gurobi.com. Accessed: 2018-07.

[HLO08] Haldimann M., Luible A., Overend M.: *Structural use of glass*, vol. 10. International Association for Bridge and Structural Engineering, Zürich, Switzerland, 2008.

[JTPSH15] Jakob W., Tarini M., Panozzo D., Sorkine-Hornung O.: Instant field-aligned meshes. *ACM Transactions on Graphics 34*, 6 (October 2015), 189:1–189:15. https://doi.org/10.1145/2816795.2818078.

[JTSW17] Jiang C., Tang C., Seidel H.-P., Wonka P.: Design and volume optimization of space structures. *ACM Transactions on Graphics 36*, 4 (July 2017), 159:1–159:14. https://doi.org/10.1145/3072959.3073619.

[KPWP17] Kilian M., Pellis D., Wallner J., Pottmann H.: Material-minimizing forms and structures. *ACM Transactions on Graphics 36*, 6 (November 2017), 173:1–173:12. https://doi.org/10.1145/3130800.3130827.

[Lou11] Louter C.: *Fragile Yet Ductile: Structural Aspects of Reinforced Glass Beams*. PhD thesis, TU Delft, 2011. URL: http://resolver.tudelft.nl/uuid:15375137-d9f6-456d-a4de-df14d167a2d2. Accessed: 2018-06.

[LPS*13] Liu Y., Pan H., Snyder J., Wang W., Guo B.: Computing self-supporting surfaces by regular triangulation. *ACM Transactions on Graphics 32*, 4 (July 2013), 92:1–92:10. https://doi.org/10.1145/2461912.2461927.

[LW00] Ludwig J. J., Weiler H.-U.: Tragstrukturen aus glas am beispiel einer ganzglastonne - schalenkonstruktion ohne tragende stahlunterkonstruktion am maximilianmuseum in augsburg. *Bautechnik 77*, 4 (2000), 246–249. https://doi.org/10.1002/bate.200001880.

[MAT18] MATLAB: *version 9.4.0.813654 (R2018a)*. The MathWorks Inc., Natick, MA, 2018.

[MCB15] Martens K., Caspeele R., Belis J.: Development of composite glass beams—A review. *Engineering Structures 101* (2015), 1–15. https://doi.org/10.1016/j.engstruct.2015.07.006.

[MCB16] Martens K., Caspeele R., Belis J.: Development of reinforced and posttensioned glass beams: Review of experimental research. *Journal of Structural Engineering 142*, 5 (2016), 04015173. https://doi.org/10.1061/(ASCE)ST.1943-541X.0001453.

[MDSB03] Meyer M., Desbrun M., Schröder P., Barr A. H.: Discrete differential-geometry operators for triangulated 2-manifolds. In *Visualization and Mathematics III* (Berlin, Heidelberg, 2003), H.-C. Hege and K. Polthier (Eds.), Springer, Berlin, Heidelberg, pp. 35–57.

[Naw00] Nawy E. G.: *Prestressed Concrete: A Fundamental Approach*. Prentice Hall, Upper Saddle River, NJ, 2000.

[OKF08] Ogawa T., Kato S., Fujimoto M.: Buckling load of elliptic and hyperbolic paraboloidal steel single-layer reticulated shells of rectangular plan. *Journal of the International Association for Shell and Spatial Structures 49*, 1 (2008), 21–36. URL: https://www.ingentaconnect.com/content/iass/jiass/2008/00000049/00000001/art00002.

[OR96] Otto F., Rash B.: *Finding Form*. Edition Alex Menges, Stuttgart, 1996.

[PBSH13] Panozzo D., Block P., Sorkine-Hornung O.: Designing unreinforced masonry models. *ACM Transaction on Graphics 32*, 4 (July 2013), 91:1–91:12. https://doi.org/10.1145/2461912.2461958.

[PJH*15] Pottmann H., Jiang C., Höbinger M., Wang J., Bompas P., Wallner J.: Cell packing structures. *Computer-Aided Design 60* (2015), 70–83. https://doi.org/10.1016/j.cad.2014.02.009.

[PLW*07] Pottmann H., Liu Y., Wallner J., Bobenko A., Wang W.: Geometry of multi-layer freeform structures for architecture. *ACM Transactions on Graphics 26*, 3 (July 2007). https://doi.org/10.1145/1276377.1276458.

[PTP*15] Pietroni N., Tonelli D., Puppo E., Froli M., Scopigno R., Cignoni P.: Statics aware grid shells. *Computer Graphics Forum 34*, 2 (May 2015), 627–641. https://doi.org/10.1111/cgf.12590.

[PTV*17] Pietroni N., Tarini M., Vaxman A., Panozzo D., Cignoni P.: Position-based tensegrity design. *ACM Transactions on Graphics 36*, 6 (November 2017), 172:1–172:14. https://doi.org/10.1145/3130800.3130809.

[RqBJ13] Ruo-qiang F., Bin Y., Jihong Y.: Stability of lamella cylinder cable-braced grid shells. *Journal of Constructional Steel Research 88* (2013), 220–230. https://doi.org/10.1016/j.jcsr.2013.05.019.

[Sob07] Sobek W.: Strutture in vetro. *Archi: Rivista Svizzera di Architettura, Ingegneria e Urbanistica, Swiss Review of Architecture, Engineering and Urban Planning*. Casagrande, Bellinzona (2007), pp. 24–31.

[SS96] Schlaich J., Schober H.: Glass-covered grid-shells. *Structural Engineering International 6*, 2 (1996), 88–90. https://doi.org/10.2749/101686696780495716.

[SS10] Singh M., Schaefer S.: Triangle surfaces with discrete equivalence classes. *ACM Transactions on Graphics 29*, 4 (July 2010), 46:1–46:7. https://doi.org/10.1145/1778765.1778783.

[Tac13] Tachi T.: Interactive freeform design of tensegrity. In *Advances in Architectural Geometry 2012* (Vienna, 2013), L. Hesselgren, S. Sharma, J. Wallner, N. Baldassini, P. Bompas and J. Raynaud (Eds.), Springer, Vienna, pp. 259–268.

[TP03] Tibert A., Pellegrino S.: Review of form-finding methods for tensegrity structures. *International Journal of Space Structures 18*, 4 (2003), 209–223. https://doi.org/10.1260/026635103322987940.

[TPP*16] Tonelli D., Pietroni N., Puppo E., Froli M., Cignoni P., Amendola G., Scopigno R.: Stability of statics aware voronoi grid-shells. *Engineering Structures 116* (2016), 70–82. https://doi.org/10.1016/j.engstruct.2016.02.049.

[TSG*14] Tang C., Sun X., Gomes A., Wallner J., Pottmann H.: Form-finding with polyhedral meshes made simple. *ACM Transactions on Graphics 33*, 4 (July 2014), 70:1–70:9. https://doi.org/10.1145/2601097.2601213.

[VHWP12] Vouga E., Höbinger M., Wallner J., Pottmann H.: Design of self-supporting surfaces. *ACM Transactions on Graphics 31*, 4 (July 2012), 87:1–87:11. https://doi.org/10.1145/2185520.2185583.

[WOD09] Whiting E., Ochsendorf J., Durand F.: Procedural modeling of structurally-sound masonry buildings. *ACM Transactions on Graphics 28*, 5 (December 2009), 112:1–112:9. https://doi.org/10.1145/1618452.1618458.

[WSW*12] Whiting E., Shin H., Wang R., Ochsendorf J., Durand F.: Structural optimization of 3d masonry buildings. *ACM Transactions on Graphics 31*, 6 (November 2012), 159:1–159:11. https://doi.org/10.1145/2366145.2366178.

[ZCBK12] Zimmer H., Campen M., Bommes D., Kobbelt L.: Rationalization of triangle-based point-folding structures. *Computer Graphics Forum 31*, 2pt3 (2012), 611–620. https://doi.org/10.1111/j.1467-8659.2012.03040.x.